Polar Meteorol. Glaciol., **13**, 111–122, 1999

Scientific Note

PERTURBATIONS OF SOLAR FLUX IN THE ANTARCTIC ATMOSPHERE-SNOW SYSTEM DUE TO VOLCANIC ASH AEROSOL AND CLOUD

Masahiro HORI[1], Teruo AOKI[2], Tadao AOKI[2], Masashi FUKABORI[2] and Akihiro UCHIYAMA[2]

[1] *National Space Development Agency of Japan, 1-9-9, Roppongi, Minato-ku, Tokyo 106-0032*
[2] *Meteorological Research Institute, 1-1, Nagamine, Tsukuba 305-0052*

Abstract: To examine the effects of volcanic ash aerosol and cloud cover on the shortwave radiation budget in the Antarctic atmosphere-snow system, solar radiation net flux at the top of the atmosphere (TOA) and the snow surface (SWS) are calculated by using a radiative transfer model based on the doubling-adding method. The calculations show that due to introduction of volcanic ash aerosol into the stratosphere, the net flux at SWS decreases and the net flux at TOA increases compared with the non-aerosol scenario. As a result, the atmosphere-subsystem (ATM) between TOA and SWS is heated due to absorption of solar radiation by the aerosol. On the other hand, cloud cover reduces the net flux at TOA and SWS considerably, and heats ATM at the solar zenith angle (θ_0) $< 64^\circ$ and cools it at $\theta_0 > 64^\circ$.

1. Introduction

Antarctica plays an important role in the earth climate system as a heat sink where emission of thermal (longwave) radiation always exceeds absorption of solar (shortwave) radiation and thus radiative net flux is always negative. It is necessary for the study of earth radiation budget to understand all of the radiative processes in the Antarctic atmosphere-snow system. In addition to snow and ice covering the Antarctic surface, cloud cover in the atmosphere also plays an important role in the radiative processes in the system through reflection of solar radiation and absorption and emission of thermal radiation. However, it is still difficult to estimate qualitatively and quantitatively the cloud radiative effects on the earth radiation budget in Antarctica, because spectral reflectance of cloud and snow are quite similar and thus methods to estimate their radiative effects, for example remote sensing by satellite, cannot discriminate accurately between cloudy area and snow covered area.

An other type of event which can have large impact on the radiative processes in the Antarctic atmosphere-snow system is volcanic eruption. Volcanic eruption introduces large amounts of volcanic ash and SO_2 gas into the stratosphere. The introduction of volcanic ash causes a significant increase of aerosol optical depth for a few months immediately after the eruption. Introduced SO_2 gas is converted to fresh H_2SO_4/H_2O aerosols in the stratosphere, which also causes following long term enhancement of

aerosol optical depth for a few years. In cases of the eruptions of both Cerro Hudson in Chile and Mt. Pinatubo in the Philippines in 1991, weekly 0.5μm aerosol optical thicknesses at several stations in Antarctica increased to 0.3, about 10 times the background level, for several months after the eruption, and then the still high level of optical thickness of about 0.1 lasted for several years (HERBER *et al.*, 1996). Thus the effect of the volcanic aerosol on the radiation budget is not negligible.

In order to understand the roles of volcanic ash aerosol and cloud in the Antarctic atmosphere-snow system and to estimate their radiation effects, we have investigated their effects on radiative processes by means of numerical simulations. In this study we estimate the effects of volcanic ash aerosol often observed just after eruptions and also that of tropospheric cloud cover on the solar radiation net flux at two boundaries, the top of the atmosphere and the snow surface, and on the solar radiation budget in the atmosphere-subsystem, by using a radiative transfer model which takes account of only solar radiation in the spectral range between 0.3 and 3.0μm. Radiative effects in the thermal radiation range are also important particularly for clouds, but the simulation is restricted to the solar radiation.

2. Simulation

2.1. *Radiative transfer model*

Radiative flux at the top of the atmosphere and the snow surface is calculated by using a radiative transfer model based on the doubling and adding method. In this model the atmosphere is assumed to be plane-parallel and to be composed of 13 layers, and one snow layer having semi-infinite optical depth ($\tau=3200$ at $\lambda=0.5\mu$m) is considered just below the bottom of the atmosphere (Fig. 1). The multiple scattering of light in the solar spectral range is taken into account (λ: 0.325–2.975μm, 54 bands,

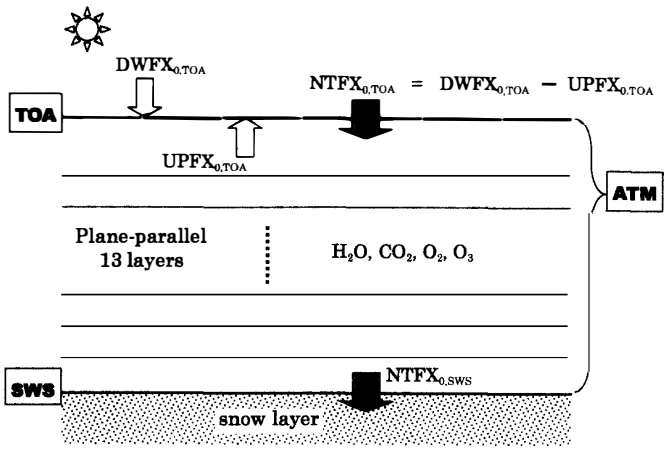

Fig. 1. Schematic of atmosphere-snow system used in the radiative transfer model. TOA denotes top of atmosphere, SWS denotes snow surface and ATM denotes atmosphere subsystem. Calculated solar radiation flux at each boundary is indicated by DWFX for downward flux, UPFX for upward flux. Net flux at each boundary indicated by NTFX is defined as the difference between DWFX and UPFX.

$\Delta\lambda = 0.05\,\mu$m) and H_2O, CO_2, O_2 and O_3 gaseous absorption in the spectral range is also considered according to the subarctic winter model atmosphere of AFGL (ANDERSON *et al.*, 1986). It is assumed that snow grains in the snow layer are composed of spherical particles of ice, and their sizes are distributed in a gamma-type distribution ($\nu_{eff} = 0.125$). Two effective radius (r_{eff}) cases of 50, 1000 μm and fourteen solar zenith angle (θ_0) cases of 5.9, 13.5, 21.1, 28.6, 36.0, 43.2, 50.1, 56.8, 63.1, 68.9, 74.3, 79.0, 83.0 and 86.1° have been calculated. The complex refractive index of ice for the solar radiation spectral range was taken from the paper of WARREN (1984), who compiles the optical constants of ice from the ultraviolet (45 nm) to the microwave (8.6 m). In his paper methods to obtain the optical constants of ice for each spectral range and their reliabilities are described. Further detail of the radiative transfer model is given by AOKI *et al.* (1999).

2.2. Scenarios

The solar radiation net flux is calculated for three scenarios; (1) clear scenario, (2) aerosol scenario, (3) cloud scenario. In the clear scenario, only Rayleigh scattering by air molecules and absorption by gases are taken into account. The aerosol scenario assumes that volcanic ash aerosol is introduced into the stratosphere. The cloud scenario assumes cloud occurs in the lower troposphere. Simulations assuming these latter two scenarios are carried out to estimate the radiative effects of both volcanic ash aerosol and cloud on the net flux by comparing with the clear scenario.

2.2.1. Aerosol

In the aerosol scenario, sulfuric acid aerosol ($\tau_a = 0.02$ at $\lambda = 0.5\,\mu$m) is assumed to be always in the troposphere (0–5 km altitude) as a background aerosol and two cases of volcanic ash aerosol ($\tau_a = 0.08$, 0.28 at $\lambda = 0.5\,\mu$m) are assumed to be introduced into the stratosphere (10–25 km). As a real background condition, sulfuric acid aerosol is in the stratosphere, too. However, its optical depth is negligible compared with that of volcanic ash aerosol after the eruption. In this simulation to estimate the effect of only volcanic ash aerosol, background sulfuric acid aerosol in the stratosphere is not considered. Therefore three cases of aerosol optical depth at $\lambda = 0.5\,\mu$m are calculated as follows; $\tau_a = 0.02$: only tropospheric background aerosol, $\tau_a = 0.1$: background + optically thin volcanic ash aerosol, $\tau_a = 0.3$: background + optically thick volcanic ash aerosol. The last case was observed at Antarctic stations after the eruptions of Cerro Hudson and Mt. Pinatubo, as mentioned in Section 1. Size distributions of both background and volcanic ash aerosols are assumed to be represented by the log-normal distributions with effective radii of $r_{eff} = 0.1\,\mu$m (geometric mean radius: $r_{gN} = 0.057\,\mu$m) for background aerosol and $r_{eff} = 0.32\,\mu$m ($r_{gN} = 0.23\,\mu$m) for volcanic ash aerosol, based on the observation results (SHAW, 1982; ITO, 1989). The complex refractive index of sulfuric acid and volcanic ash were taken from AFGL (1985).

2.2.2. Cloud

It is assumed that cloud occurs at the height of 2–3 km in the troposphere. We calculate three cases of cloud optical depth at $\lambda = 0.5\,\mu$m of $\tau_c = 2.5$, 5, 10. Cloud droplets are assumed to be spheres composed of water with the size distribution given by DEIRMENDJIAN (1964)'s cloud model ($r_{eff} = 5\,\mu$m). The complex refractive index of water was taken from AFGL (1985).

2.3. Solar radiation flux at each boundary

To estimate the effects of volcanic ash aerosol and cloud on the shortwave radiation budget, we calculate the downward flux (DWFX) and the upward flux (UPFX) of solar radiation at the top of the atmosphere (TOA) and the snow surface (SWS) for each scenario by using the radiative transfer model. Net fluxes (NTFX) at TOA and SWS are calculated as the difference between DWFX and UPFX for each scenario as follows,

$$\mathrm{NTFX}_{\mathrm{scnr,\,bnd}} = \mathrm{DWFX}_{\mathrm{scnr,\,bnd}} - \mathrm{UPFX}_{\mathrm{scnr,\,bnd}}, \tag{1}$$

where the subscript "bnd" means a boundary of the atmosphere-snow system such as TOA and SWS and "scnr" means aerosol or cloud scenario. NTFX is defined to have positive values when DWFX is larger than UPFX. Then, perturbations of the net flux (ΔNTFX) at TOA and SWS due to volcanic ash aerosol or cloud are also calculated by the following equation, which gives the difference in NTFX between aerosol or cloud scenario and clear scenario,

$$\Delta\mathrm{NTFX}_{\mathrm{scnr,\,bnd}} = \mathrm{NTFX}_{\mathrm{scnr,\,bnd}} - \mathrm{NTFX}_{0,\,\mathrm{bnd}}, \tag{2}$$

where the subscript "0" means the clear scenario. In this study, the perturbation of the net flux in the atmosphere sub-system which is defined as the difference in ΔNTFX between TOA and SWS is calculated as follows;

$$\Delta\mathrm{NTFX}_{\mathrm{scnr,\,ATM}} = \Delta\mathrm{NTFX}_{\mathrm{scnr,\,TOA}} - \Delta\mathrm{NTFX}_{\mathrm{scnr,\,SWS}}, \tag{3}$$

where "ATM" means atmosphere sub-system (see Fig. 1). The ΔNTFX value becomes a measure of the effect of aerosol or cloud on the radiation budget compared with the clear scenario. Positive (negative) value means heating (cooling).

3. Results and Discussion

Figures 2-1a, b show the simulated solar radiation flux (DWFX, UPFX, NTFX) at TOA and SWS respectively in case of the clear scenario calculated for snow grain size of $r_{\mathrm{eff}} = 50\,\mu$m. Figures 2-2a, b show the same results calculated for the grain size of $r_{\mathrm{eff}} = 1000\,\mu$m. As the solar zenith angle becomes larger, downward flux (DWFX) at TOA decreases because the DWFX is defined as the solar irradiance multiplied by cosine of solar zenith angle ($F_0 \times \cos\theta_0$). As the DWFX is the input energy for the atmosphere-snow system, UPFX and NTFX in the same figures show the same dependence on solar zenith angle. Both Figs. 2-1 and 2-2 indicate that DWFX at TOA is larger than that at SWS, on the other hand UPFX at TOA is smaller than that at SWS. This is due to the Rayleigh scattering by air molecules and absorption by atmospheric gases such as H_2O, CO_2, O_2 and O_3, which decrease the transmitted downward flux (DWFX) at SWS compared with TOA and also decrease the reflected upward flux (UPFX) at TOA. YAMANOUCHI (1983) observed global solar radiation under clear sky condition at Mizuho Station, East Antarctica where aerosol optical thickness is very low. YAMANOUCHI compared the DWFX measured at Mizuho with a typical value of DWFX measured at mid-latitude by PALTRIDGE and PLATT (1976) where aerosol and water vapor concentrations are higher than in the south polar region. The result of YAMANOUCHI (1983) is also shown in Fig. 2-1b for comparison (solid line for the measured DNFX is based on the eq. (3) in YAMANOUCHI (1983)). The difference

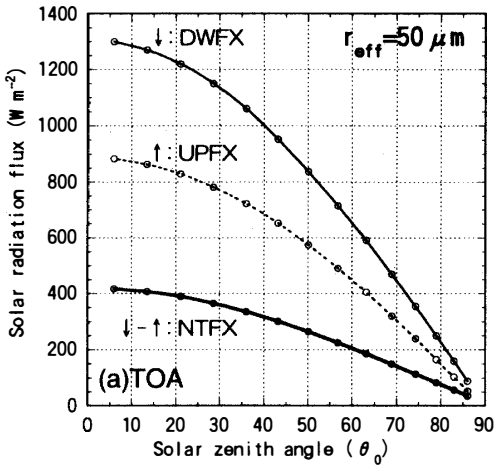

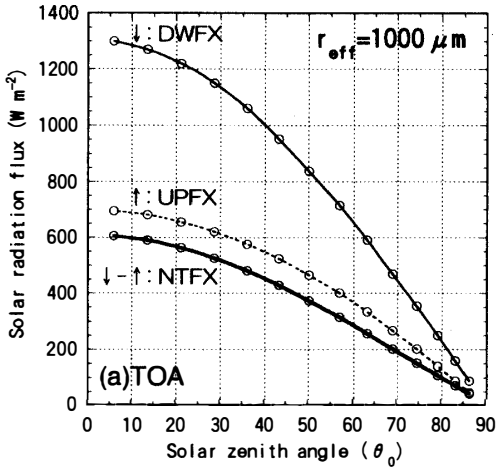

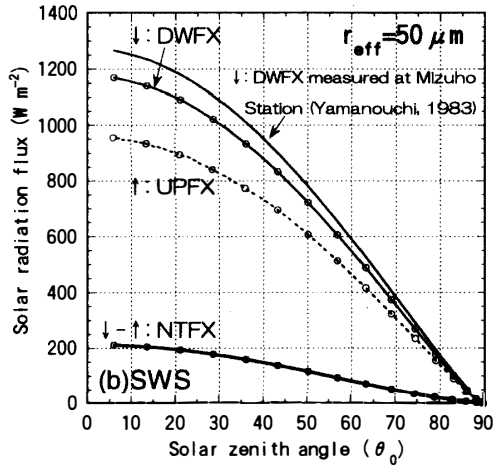

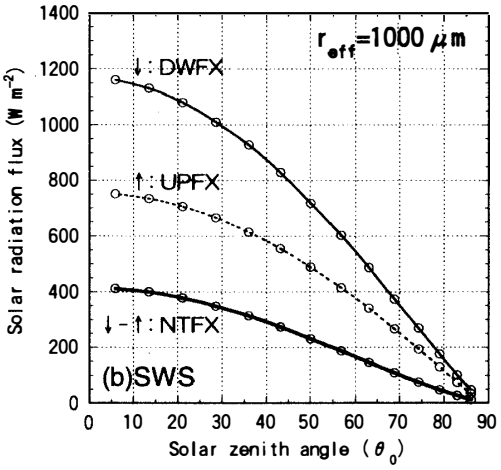

Fig. 2-1.

Fig. 2-2.

Fig. 2-1. Simulated solar radiation downward (DWFX), upward (UPFX) and net (NTFX) flux at (a) top of atmosphere (TOA) and (b) snow surface (SWS) calculated for the snow grain size of r_{eff}=50 μm. Solid line without circle in Fig. 2-1b is the DWFX measured at Mizuho Station by YAMANOUCHI (1983).

Fig. 2-2. Same as Fig. 2-1 for snow grain size of r_{eff}=1000 μm.

between the measured DWFX and the calculated values in the figure results from the difference in their location heights. Mizuho Station is located at the high altitude of 2230 m. On the other hand, this study calculates the flux at the snow surface at 0 m height. Thus the atmospheric layer above Mizuho Station is thinner than that in this calculation. As mentioned above, in the atmosphere Rayleigh scattering by air molecules and absorption by atmospheric gases reduces the transmittance to solar radiation. That is why the DNFX at Mizuho is always higher than the calculated values. In addition, the calculated DWFX (*e.g.*, about 540 Wm^{-2} at solar zenith angle of 60°) is approximately midway between the DWFX measured at Mizuho (about 590 Wm^{-2}) and that measured at mid-latitude by PALTRIDGE and PLATT (1976) (about 490 Wm^{-2}, not

shown in Fig. 2-1b). Taking account of the differences in their location heights, considering the concentrations of water vapor and the existence of aerosol in the mid-latitude case, the calculated DNFX can be considered as reasonable.

At each boundary, the upward flux (UPFX) for snow grain size of $r_{eff}=1000\mu$m (Fig. 2-2) is smaller than that for $r_{eff}=50\mu$m (Fig. 2-1) at all solar zenith angles. This is due to the dependence of snow surface albedo on snow grain size. The larger the snow grain size, the lower the snow surface albedo (WISCOMBE and WARREN, 1980). Thus a surface consisting of larger grain particles reflects less solar radiation than a surface consisting of smaller grain particles. This is why the UPFX for the case of $r_{eff}=1000\mu$m is always smaller than that for $r_{eff}=50\mu$m. In addition, the lower surface albedo for $r_{eff}=1000\mu$m reduces multiple scattering in the atmosphere, which leads to slightly lower DWFX at SWS for $r_{eff}=1000\mu$m than $r_{eff}=50\mu$m. As a result of both DWFX and UPFX the net flux (NTFX) at both TOA and SWS for $r_{eff}=50\mu$m is always lower than that for $r_{eff}=1000\mu$m. Net flux at the TOA for $r_{eff}=50\mu$m becomes about two thirds of that for $r_{eff}=1000\mu$m and net flux at the SWS for $r_{eff}=50\mu$m becomes about half of that for $r_{eff}=1000\mu$m.

Next, we compare the solar radiation net fluxes in case of the aerosol or the cloud scenario with those of the clear scenario to estimate the effect of aerosol and cloud on the net fluxes.

3.1. *Volcanic ash aerosol*

Figures 3a–c show the perturbations of radiative net flux (ΔNTFX) at TOA, SWS and ATM respectively due to the introduction of volcanic ash aerosol into the stratosphere calculated for three optical depths and for constant snow grain size ($r_{eff}=50\mu$m). The net flux for clear scenario ($NTFX_0$) is also indicated in the same figures corresponding to the right axis. In this scenario, background aerosol causes little perturbation in radiative net flux at both boundaries, TOA and SWS, and in ATM. On the other hand, volcanic ash aerosol causes positive perturbation at TOA and ATM and negative perturbation at SWS. Because volcanic ash aerosol has weak absorptivity of solar radiation in the visible wavelength region, the aerosol distributed in the stratosphere absorbs solar radiation and warms the atmosphere subsystem, particularly in the stratosphere. This leads to positive perturbation of the net flux up to about $+16.5$ Wm^{-2} (13.8% of the net flux) for $\theta_0=60^\circ$ and $\tau_a=0.3$ at ATM. Actually, in the past the stratospheric warming events caused by volcanic aerosol were observed in the lower latitude region near the equator (PARKER and BROWNSCOMBE, 1983; LABITZKE and MCCORMICK, 1992). At some locations between the equator and 30°N, stratospheric warming as high as 3.5°C was observed at 20 km altitude in September and October 1991, with 525 nm aerosol optical depth being higher than 0.1 (KINNISON *et al.*, 1994). The calculated result suggests that the same type of stratospheric warming by volcanic ash aerosol introduced by the eruptions of Cerro Hudson and Mt. Pinatubo also occurred in the Antarctic region after the aerosol was transported from lower latitude to the polar region in late 1991 and 1992. In addition, the stratospheric warming decreases the upward solar flux at TOA, which causes positive perturbation of net flux by $+13.5$ Wm^{-2} (6.6%) for $\theta_0=60^\circ$ and $\tau_a=0.3$ at TOA, and also decreases downward transmitted flux at SWS, which leads to negative perturbation of net flux by -3 Wm^{-2}

(3.8%) at SWS. Thus the effect of volcanic ash aerosol on the shortwave radiation budget at SWS is cooling, and that on TOA is heating.

Figures 4a–c are same figures as Fig. 3 except that snow grain is $r_{eff}=1000\mu m$. In the same manner as in Fig. 3, volcanic ash aerosol causes positive perturbation of radiative net flux at both ATM ($+15.5\,Wm^{-2}$ (13% of net flux) for $\theta_0=60^\circ$, $\tau_a=0.3$) and TOA ($+6.5\,Wm^{-2}$ (2.3%)) and negative perturbation at SWS ($-9\,Wm^{-2}$ (5.5 %)). Compared with the case of $r_{eff}=50\mu m$, the perturbation at TOA for $r_{eff}=1000\mu m$ is smaller and the perturbation at SWS is larger than that for $r_{eff}=50\mu m$. This is due to the following. Because the DWFX at TOA is constant, the perturbation of net flux at TOA is determined by the perturbation of UPFX. As shown in Fig. 2-1 and 2-2, UPFX for $r_{eff}=1000\mu m$ is smaller than that for $r_{eff}=50\mu m$. Thus the fraction of UPFX at TOA decreased by the aerosol for $r_{eff}=1000\mu m$ becomes smaller than that for $r_{eff}=50\mu m$. For SWS, also, UPFX for $r_{eff}=1000\mu m$ is smaller than $r_{eff}=50\mu m$; in contrast, DWFXs for both grain sizes are almost the same. Thus, the fraction of UPFX decreased by the volcanic ash aerosol for $r_{eff}=1000\mu m$ becomes smaller than that for $r_{eff}=50\mu m$, which makes the difference between DWFX and UPFX for $r_{eff}=1000\mu m$ smaller than that for $r_{eff}=50\mu m$. That is why the negative perturbation at SWS for $r_{eff}=1000\mu m$ is larger than that for $r_{eff}=50\mu m$. As a results of the decreases of NTFX at both TOA and SWS boundaries for $r_{eff}=1000\mu m$ compared with that for $r_{eff}=50\mu m$, the positive perturbation at ATM for $r_{eff}=1000\mu m$ becomes almost the same as that for $r_{eff}=50\mu m$. Thus, absorbed solar radiation in the atmosphere sub-system does not depend on the surface albedo.

3.2. Cloud

Figures 5a–c show the perturbations of the radiative net flux (ΔNTFX) at TOA, SWS and ATM respectively due to the existence of cloud calculated for three optical depths and for constant snow grain size ($r_{eff}=50\mu m$). In the same way as in Figs. 3 and 4, the net flux for the clear scenario ($NTFX_0$) is also indicated in Fig. 5. Cloud cover always decreases largely the net flux at TOA for all solar zenith angles compared with the clear scenario. In the case of $\theta_0=60^\circ$ and thick cloud ($\tau_c=10$), the negative perturbation is up to $-40\,Wm^{-2}$ (20% of net flux). The single scattering albedo of cloud droplets is larger than that of the snow grains covering the surface, mainly due to the difference of effective particle size. Thus, cloud layer scatters and reflects more solar radiation than the snow surface, and the upward solar flux at TOA in the cloud scenario becomes larger than that in the clear scenario. This is why the perturbation of the net flux at TOA becomes negative. Thus, the effect of cloud cover on the radiation budget at TOA is cooling. Perturbation of the net flux at SWS is also always negative, up to $44\,Wm^{-2}$ (55%) for $\theta_0=60^\circ$ and $\tau_c=10$. As the net flux at SWS is smaller than at TOA ($NTFX_{0,TOA}>NTFX_{0,SWS}$), the ratio of the perturbation to the net flux (ΔNTFX/NTFX) at SWS becomes even larger than that at TOA. This negative perturbation at SWS is partly due to the absorption of solar radiation in the near infrared region by water vapor in the cloud layer, and partly due to the low spectral albedo of the snow surface in the near infrared region (Aoki *et al.*, 1999). The absorption by water vapor in cloud decreases the transmitted downward flux in the spectral region at SWS. On the other hand, as DWFX in the infrared region at the

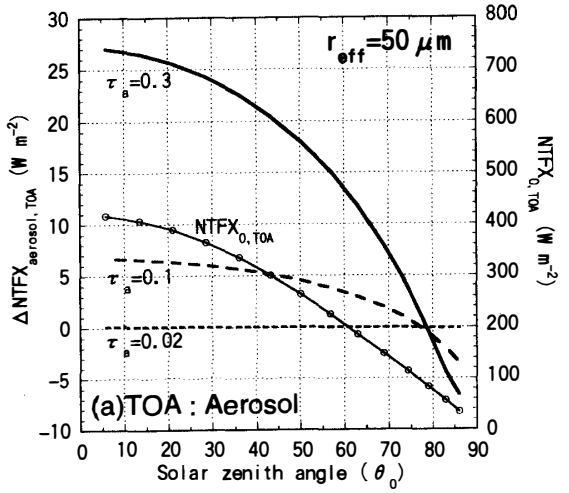

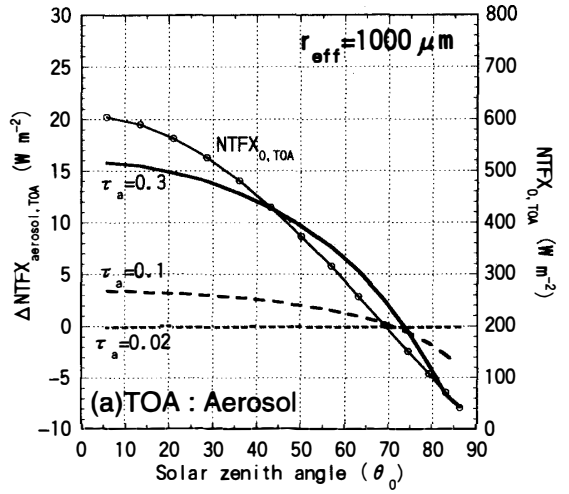

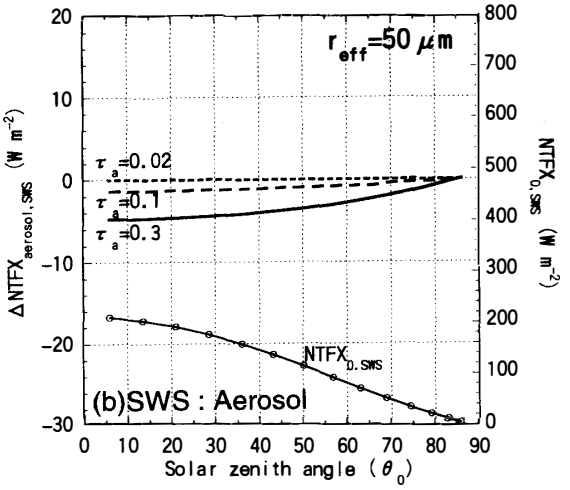

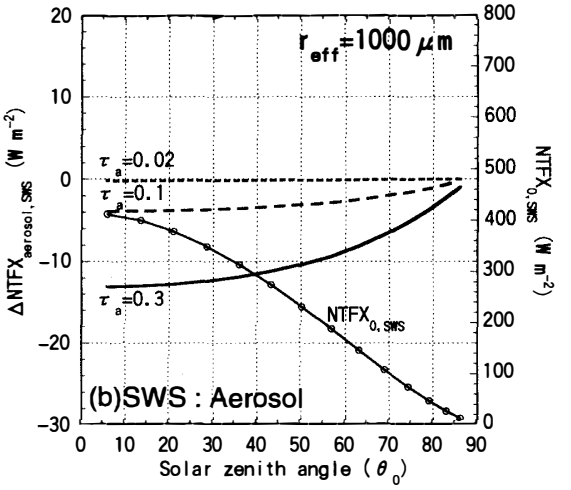

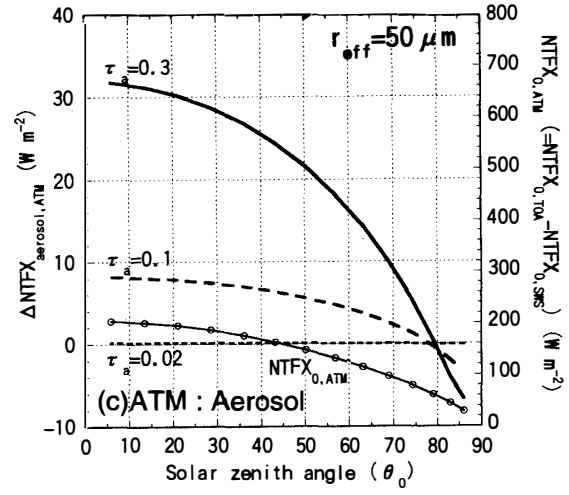

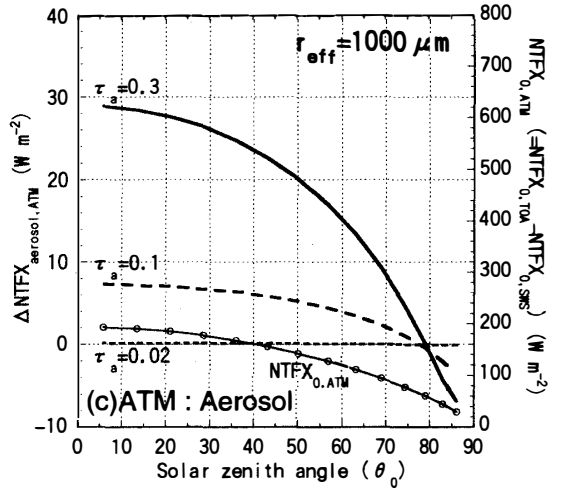

Fig. 3. *Fig. 4.*

Fig. 3. Simulated perturbations of solar net flux at (a) top of atmosphere (TOA), (b) snow surface (SWS) and (c) atmosphere subsystem (ATM) calculated for the aerosol scenario of three optical depths (τ_a=0.02, 0.1, 0.3) and snow grain size of r_{eff}=50 μm. Net flux ($NTFX_0$) for the clear scenario is also indicated in the figure corresponding to right axis.

Fig. 4. Same as Fig. 3 for snow grain size of r_{eff}=1000 μm.

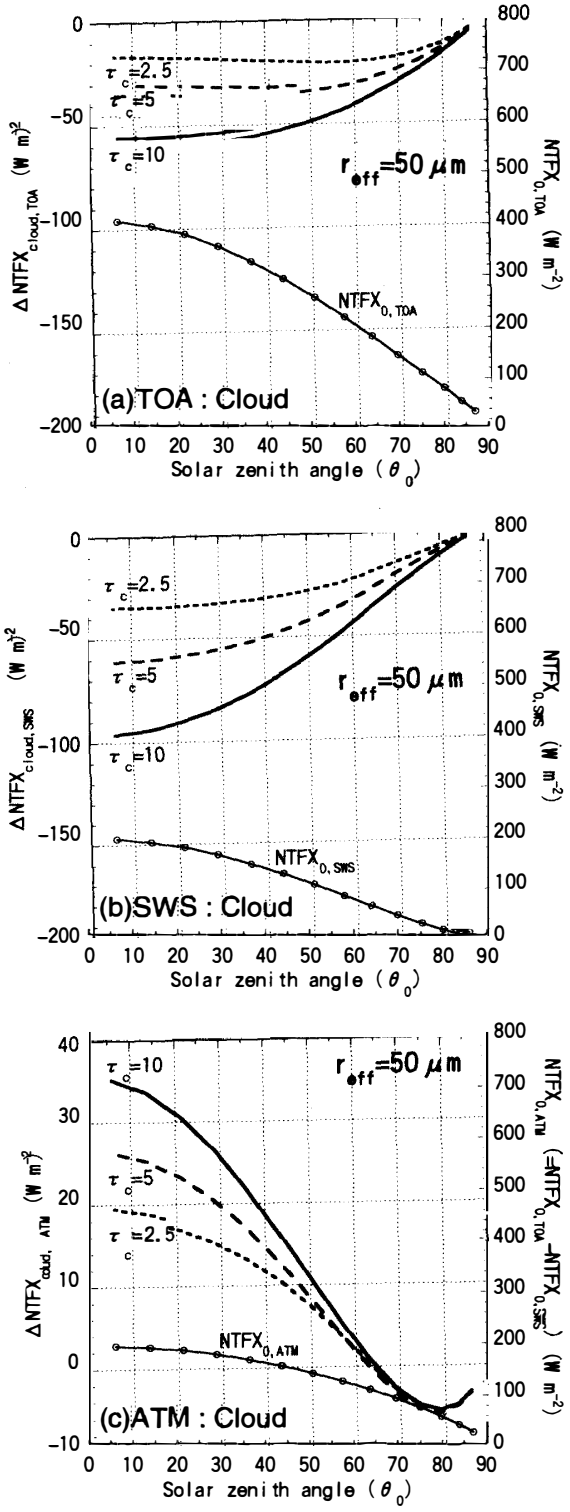

Fig. 5.

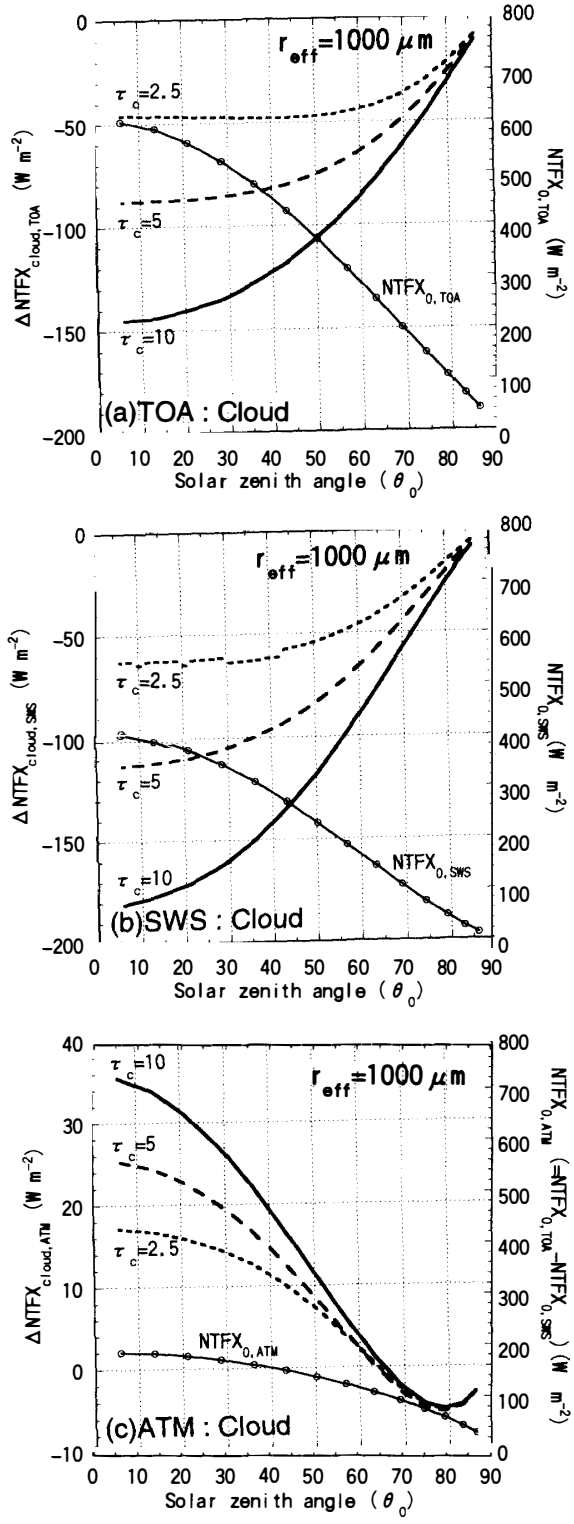

Fig. 6.

Fig. 5. Same as Fig. 3 for the cloud scenario of three optical depths (τ_c=2.5, 5, 10).

Fig. 6. Same as Fig. 5 for snow grain size of r_{eff}=1000 μm.

snow surface is already decreased in the cloud, UPFX reflected at SWS is not reduced as in the clear scenario in which UPFX is decreased due to the low spectral albedo in the near infrared region. As a result, the net flux at SWS under a cloudy sky becomes smaller than that under a clear sky. Thus, the effect of cloud cover on the snow surface is cooling.

As shown in Fig. 5c, the behavior of the perturbation of the net flux in the atmosphere sub-system is a little complicated. Reflecting the difference in the dependence of the albedo at TOA and SWS on solar zenith angle between cloud and clear scenario, at small solar zenith angle the negative perturbation of net flux at SWS exceeds the perturbation at TOA, while at large angle the perturbation at TOA exceeds the perturbation at SWS. As a result, under cloudy condition the perturbation of net flux in the ATM can become both positive (heating) and negative (cooling) depending on the solar zenith angle; that is, when the solar zenith angle is smaller than 64° the atmosphere sub-system is heated, and vice versa.

Basically above results on the perturbation of the net flux at TOA, SWS and in the ATM are consistent with the observational study of YAMANOUCHI and CHARLOCK (1995) at Syowa Station. They estimate the effect of cloud on shortwave radiation net flux at TOA, SWS and in the ATM on daily mean basis. In summer (Jan. 1988) the daily mean shortwave absorption at Syowa Station was $-54.6\,\mathrm{Wm}^{-2}$ at TOA, $-65.8\,\mathrm{Wm}^{-2}$ at SWS and $+11.2\,\mathrm{Wm}^{-2}$ in ATM. Their results show the same radiative effect (cooling) of cloud at TOA and SWS as in our calculated results, although the cloud optical depth cannot be specified. In the ATM, our result shows both heating and cooling effects depending on the solar zenith angle. At Syowa Station the daily solar zenith angle in January varies between 90° and 45°. On a daily average the calculated perturbation of the net flux in the ATM becomes slightly positive (roughly estimated as $+1.5\,\mathrm{Wm}^{-2}$). Thus, even in the atmosphere sub-system, the sign of our result is consistent with that of YAMANOUCHI and CHARLOCK. It should be noted that depending on the latitude, the sign of the daily basis perturbation in the ATM varies between positive and negative. At higher latitude than Syowa Station the cooling effect can exceed heating.

Figures 6a–c show the same figures as Fig. 5 except that the snow grain size is $r_{\mathrm{eff}} = 1000\,\mu\mathrm{m}$. In the same manner as in Fig. 5, cloud causes negative large perturbation of the net flux at both the TOA and SWS, and both positive and negative perturbation in the ATM depending on the solar zenith angle. Compared with Fig. 5, the negative perturbations at TOA and SWS for $r_{\mathrm{eff}} = 1000\,\mu\mathrm{m}$ are larger than those for the $r_{\mathrm{eff}} = 50\,\mu\mathrm{m}$ case. As mentioned in Section 3, snow surface albedo varies depending on the snow grain size, which causes a large difference in net fluxes between the $r_{\mathrm{eff}} = 50\,\mu\mathrm{m}$ and $r_{\mathrm{eff}} = 1000\,\mu\mathrm{m}$ cases (Figs. 2-1, 2-2). And the difference in snow surface albedo results in a difference in the perturbation of net flux in the aerosol scenario between Figs. 3 and 4. In the cloud scenario, also, the lower surface albedo of the $r_{\mathrm{eff}} = 1000\,\mu\mathrm{m}$ case amplifies the negative perturbation of net flux at TOA and SWS. However, it should be noted that the ratio of the perturbation to net flux (ΔNTFX/NTFX) at TOA and SWS for the $r_{\mathrm{eff}} = 1000\,\mu\mathrm{m}$ case is almost the same as for the case of $r_{\mathrm{eff}} = 50\,\mu\mathrm{m}$. For example, for the case of $\theta_0 = 60°$ and $\tau_c = 10$, ΔNTFX/NTFX ($r_{\mathrm{eff}} = 50\,\mu\mathrm{m}$) at the TOA and SWS are 0.2 and 0.55, respectively, and ΔNTFX/NTFX ($r_{\mathrm{eff}} = 1000\,\mu\mathrm{m}$) at the TOA and SWS

are 0.3 and 0.55, respectively. Thus almost the same percentages of the net flux are changed by cloud cover in both the $r_{eff}=50\mu$m and $r_{eff}=1000\mu$m cases.

4. Summary

In this study we calculated the perturbations of solar radiation net flux at the top of the atmosphere, at the snow surface and in the atmosphere to estimate the effect of volcanic ash aerosol and cloud cover on the shortwave radiation budget in the Antarctic atmosphere-snow system. Qualitative results are summarized in Table 1. Volcanic

Table 1. Signs of radiative effects of volcanic ash aerosol and cloud on the shortwave net flux at the top of the atmosphere (TOA), snow covered surface (SWS) and in the atmosphere (ATM) compared with the clear sky. "+" and "−" denote heating and cooling effects, respectively.

Boundary or sub-system	Volcanic ash aerosol	Cloud
TOA	+	−
SWS	−	−
ATM	+	+($5.9<\theta_0<64°$) −($64<\theta_0<86.1°$) θ_0: solar zenith angle

ash aerosol causes positive perturbations (heating) at the TOA and in the ATM and negative perturbation (cooling) at the SWS due to absorption of solar radiation by the aerosol. On the other hand, cloud cover causes large negative perturbations at the TOA and SWS, and causes both positive and negative perturbation in the ATM depending on the solar zenith angle. This latter perturbation in the ATM becomes slightly positive on a daily basis at Syowa Station. The simulated results are consistent with past observation results.

References

AFGL (1985): Handbook of geophysics and the space environment. Air Force Geophysics Laboratory, Hanscom, MA.

ANDERSON, G.P., CLOUGH, S.A., KNEIZYS, F.X., CHETWYND, J.H. and SHETTLE, E.P. (1986): AFGL atmospheric constituent profiles (0–120 km). AFGL-TR-86-0110, Air Force Geophysics Laboratory, Hanscom, MA.

AOKI, Te., AOKI, Ta., FUKABORI, M. and UCHIYAMA, A. (1999): Numerical simulation of the atmospheric effects on snow albedo with a multiple scattering radiative transfer model for the atmosphere-snow system. J. Meteorol. Soc. Jpn., **77**, 595–614.

DEIRMENDJIAN, D. (1964): Scattering and polarization properties of water clouds and hazes in the visible and infrared. Appl. Opt., **3**, 187–196.

HERBER, A., THOMASON, L.W., DETHLOFF, K., VITERBO, P., RADIONOV, V.F. and LEITERER, U. (1996): Volcanic perturbation of the atmosphere in both polar regions: 1991–1994. J. Geophys. Res., **101**, 3921–3928.

ITO, T. (1989): Antarctic submicron aerosols and longrange transport of pollutants. Ambio, **18**, 34–41.

KINNISON, D.E., GRANT, K.E., CONNEL, P.S., ROTMAN, D.A. and WUEBBLES, D.J. (1994): The chemical and radiative effects of the Mount Pinatubo eruption. J. Geophys. Res., **99**, 25705–25731.

LABITZKE, K. and MCCORMICK, M.P. (1992): Stratospheric temperature increases due to Pinatubo aerosols. Geophys. Res. Lett., **19**, 207–210.

PALTRIDGE, G.W. and PLATT, C.M.R. (1976): Radiative processes in meteorology and climatology. New York, Elsevier, 318 p. (Developments in Atmospheric Science, 5).

PARKER, D.E. and BROWNSCOMBE, J.L. (1983): Stratospheric warming following the El Chichon volcanic eruption. Nature, **301**, 406–408.

SHAW, G.E. (1982): Atmospheric turbidity in the polar regions. J. Appl. Metorol., **21**, 1080–1088.

WARREN, S.G. (1984): Optical constants of ice from the ultraviolet to the microwave. Appl. Opt., **23**, 1206–1225.

WISCOMBE, W.J. and WARREN, S.G. (1980): A model for the spectral albedo of snow. I: Pure snow. J. Atom. Sci., **37**, 2712–2733.

YAMANOUCHI, T. (1983): Variations of incident solar flux and snow albedo on the solar zenith angle and cloud cover, at Mizuho Station, Antarctica. J. Meteorol. Soc. Jpn., **61**, 879–893.

YAMANOUCHI, T. and CHARLOCK, T.P. (1995): Comparison of radiation budget at the TOA and surface in the Antarctic from ERBE and ground surface measurements. J. Clim., **8**, 3109–3120.

(Received January 29, 1999; Revised manuscript accepted August 4, 1999)